Dalton Transactions

Accepted Manuscript

ROYAL SOCIETY OF CHEMISTRY

www.rsc.org/dalton

Journal Name

RSCPublishing

ARTICLE

DFT examination of rare α-$SiMe_3$ abstraction in $Ta(NMe_2)_4[N(SiMe_3)_2]$: Formation of the imide compound $Ta(=NSiMe_3)(NMe_2)_3$ and its trapping to give guanidinate imides

Cite this: DOI: 10.1039/xoxx ooooox

Michael G. Richmond,*[a] and Zi-Ling Xue[b]

Received ooth ay 2014,

[a]Department of Chemistry, The University of North Texas, Denton, TX 76203, USA. [b]Department of Chemistry, The University of Tennessee, Knoxville, TN 37996, USA.

www.rsc.org/

A density functional theory (DFT) investigation on the formation of $Ta(=NSiMe_3)(NMe_2)_3$ (**B**) and Me_3SiNMe_2 (**C**) from $Ta(NMe_2)_4[N(SiMe_3)_2]$ is reported. Three different ground-state minima are computed for $Ta(NMe_2)_4[N(SiMe_3)_2]$, and of these only the stereoisomer based on a square pyramid (**A2**) with an apical $N(SiMe_3)_2$ group undergoes α-elimination to give $Ta(=NSiMe_3)(NMe_2)_3$ (**B**) and Me_3SiNMe_2 (**C**). The barrier computed for the concerted α-elimination is in agreement with the results from our earlier experimental study. The thermodynamics for the monomer-dimer equilibrium involving $Ta(=NSiMe_3)(NMe_2)_3$ (**B**) has been computationally evaluated, and the preference for the dimeric form of the compound is discussed relative to the Nugent imide derivative $Ta(=NCMe_3)(NMe_2)_3$, which exists as a monomer. The trapping of the intermediate **B** by the heterocumulene MeN=C=NMe has been modeled, and the mechanism involved in the formation of the guanidinate-based insertion products $Ta(NSiMe_3)(NMe_2)_2[MeNC(NMe_2)NMe]$ (**G1**) and $Ta(NSiMe_3)(NMe_2)[MeNC(NMe_2)NMe]_2$ (**I**) is presented.

Introduction

Transition metal imide complexes contain metal-nitrogen multiple bonds. They are typically prepared by intermolecular and intramolecular imidations.[1-27] Intermolecular imidations, which are more common, involve reactions with primary amines, imines, nitriles, and other nitrogen-containing compounds.[1-21] For example, reactions of OsO_4 with $^tBuNH_2$, $MoOCl_2(S_2CNEt_2)_2$ with $PhN=PPh_3$, and $ReOCl_3(PPh_3)_2$ with PhN=CHNHPh yield $^tBuN=OsO_3$,[18] $PhN=MoCl_2(S_2CNEt_2)_2$[19] and $PhN=ReCl_3(PPh_3)_2$[20] respectively. In intramolecular imidation, 1,2–Me_3SiCl elimination or interligand transfer (Scheme 1) gives the imide ligand in the complexes.[1-18,22,23] $Me_3SiN=TiCl_2(py)_2$ has been prepared through α-$SiMe_3$ abstraction by a chloride ligand in the reaction of pyridine with $TiCl_3[N(SiMe_3)_2]$.[21] When 3 equiv of $NaN(SiMe_3)_2$ reacts with $VOCl_3$, $SiMe_3$ migration to the oxo ligand affords the imide $Me_3SiN=V(OSiMe_3)[N(SiMe_3)_2]_2$.[22]

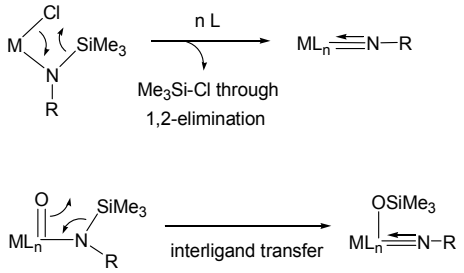

Scheme 1. Intramolecular imidation reactions.[1]

Intramolecualr imidation through α-$SiMe_3$ abstraction by an amide ligand is rare. Herrmann and Baratta have reported that, when the Nb and Ta complexes **1a-b** were irradiated at ambient temperature with a mercury lamp for 12 and 10 h, respectively, the cleavage of the Si-N bonds in the complexes occurred (Scheme 2), yielding the imide complexes **2a-b**.[26] Xue and coworkers recently reported that the amide complex $Ta(NMe_2)_4[N(SiMe_3)_2]$ undergoes spontaneous, thermal α-$SiMe_3$ abstraction by an amide ligand yielding Me_3SiNMe_2 (**C**) and the imide **B** which was observed as its dimer **D** (Scheme 3).[27,28] Kinetic studies of the thermal α-$SiMe_3$ abstraction in $Ta(NMe_2)_4[N(SiMe_3)_2]$ showed that it follows first-order kinetics, probably through a cyclic transition state, with the activation parameters: $\Delta H^{\neq}$ = 21.3(1.0) kcal/mol, $\Delta S^{\neq}$ = -17(2) eu and $\Delta G^{\neq}_{343K}$ = 27.1(1.7) kcal/mol.[27] In the presence of carbodiimides RN=C=NR (R = Cy, ^{i}Pr), **B** was trapped as guanidinate imides such as $Ta(NMe_2)_2(=NSiMe_3)[CyNC(NMe_2)NCy]$ (**3**) and $Ta(NMe_2)(=NSiMe_3)[CyNC(NMe_2)NCy]_2$ (**4**). Since the formation of **B** is a rare example of the α-$SiMe_3$ abstraction by an amide ligand to give an imide, we have conducted DFT calculations to study the reaction and subsequent capture of **B** in Scheme 3. The model compound MeN=C=NMe (**E**) was used in the capture reactions to form the guanidinate imides $Ta(NSiMe_3)(NMe_2)_2[MeNC(NMe_2)NMe]$ (**G1**) and $Ta(NSiMe_3)(NMe_2)[MeNC(NMe_2)NMe]_2$ (**I**). Our results are reported here

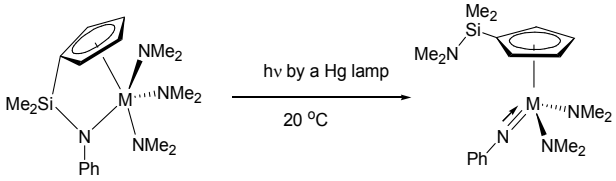

M = Nb, **1a**; Ta, **1b** M = Nb, **2a**; Ta, **2b**

Scheme 2. Formation of imides **2a-b** via photochemical cleavage of Si-N bonds.[26]

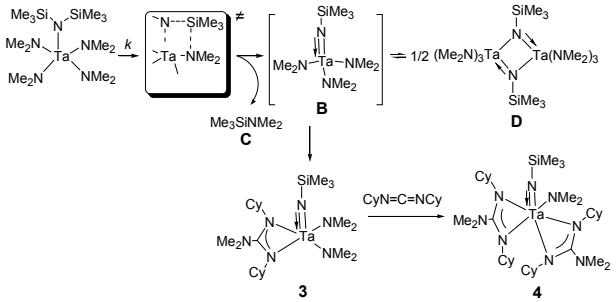

Scheme 3. Formation of the imide complex **D** and guanidinate imides **3** and **4**.[27]

Experimental Section

Computational Methodology and Modeling Details

All calculations were performed with the hybrid meta DFT functional M06, as implemented by the Gaussian 09 program package.[29] This functional provided the best agreement of theory with the available crystal structures and experimental data.[30] B3LYP calculations[31] were also performed, but these calculations did not accurately reproduce the equilibrium between monomer B and dimer D. The B3LYP data have been deposited as electronic supplementary information (ESI). The Ta atoms were described by Stuttgart-Dresden effective core potentials (ecp) and SDD basis set, while the 6-31G(d') basis set was employed for the remaining atoms.

The input data for compounds $[Ta(NMe_2)_3(\mu\text{-}NSiMe_3)_2]_2$ (**D**) and $Ta(NSiMe_3)(NMe_2)[MeNC(NMe_2)NMe]_2$ (**I**) were taken from the X-ray diffraction structures. While CyN=C=NCy was employed as the carbodiimide in the initial study, the cyclohexyl groups were replaced by methyl groups here in order to facilitate the geometry optimizations. All reported geometries were fully optimized and evaluated for the correct number of imaginary frequencies through calculation of the vibrational frequencies, using the analytical Hessian. Zero imaginary frequencies (positive eigenvalues) correspond to an intermediate or minimum, and species having an imaginary frequency (negative eigenvalue) designate a transition state. All transition states on the potential energy surface were evaluated by IRC calculations, in order to establish the reactant and product species associated with each transition-state structure. The computed frequencies were used to make zero-point and thermal corrections to the electronic energies, and standard-state corrections were added to all species to convert concentrations from 1 atm to 1 M, as outlined in the treatise by Cramer.[32] The Wiberg bond indices were computed using Weinhold's natural bond orbital (NBO) program, as executed by Gaussian 09.[33,34] The geometry-optimized structures have been drawn with the *JIMP*2 molecular visualization and manipulation program.[35]

Results and Discussion

Geometry Optimization of $Ta(NMe_2)_4[N(SiMe_3)_2]$ and Stereospecific α-Elimination

The mixed amide complex $Ta(NMe_2)_4[N(SiMe_3)_2]$ is prepared from the reaction of $TaCl(NMe_2)_4$ with $LiN(SiMe_3)_2$, and the product has been characterized by NMR spectroscopy and combustion analysis.[27] Unfortunately, the molecular structure of $Ta(NMe_2)_4[N(SiMe_3)_2]$ remains unknown due to its limited stability and the inability to grow single crystals suitable for X-ray diffraction analysis.[28] $Ta(NMe_2)_4[N(SiMe_3)_2]$ may be viewed as an ML_5 compound with a Ta(V) center. Such d^0 compounds are highly fluxional in solution as a result of low-energy Berry pseudorotations,[36] and this fluxionality hinders the identification of the preferred ground-state structure in this genre of tantalum compounds. Accordingly, the relative stability of the different possible trigonal-bipyramidal and square-pyramidal isomers available to $Ta(NMe_2)_4[N(SiMe_3)_2]$ were evaluated by DFT calculations. Figure 1 shows the optimized structures for the three different minima computed

for $Ta(NMe_2)_4[N(SiMe_3)_2]$. Of these minima, species **A1** is thermodynamically favored. **A1** exhibits a trigonal-bipyramidal (tbp) geometry with the larger $N(SiMe_3)_2$ ligand occupying one of the equatorial sites in keeping with the tenets of valence shell electron pair repulsion (VSEPR) theory.[37] The related tbp isomer with an axially disposed $N(SiMe_3)_2$ group lies 4.7 kcal/mol above **A1**. Of the two possible square-pyramidal isomers, the one having an apical $N(SiMe_3)_2$ group, species **A2**, was computed as a stable minimum. The alternative isomer based on a square pyramid with a basal $N(SiMe_3)_2$ ligand is prohibitively crowded, and the DFT optimizations either failed or collapsed to **A1**.

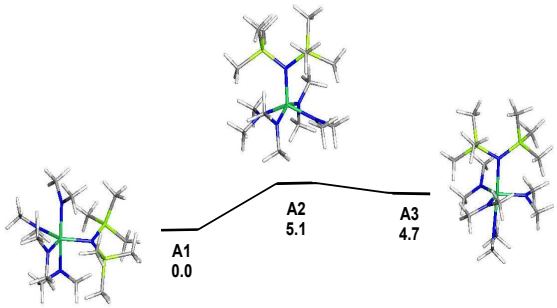

Figure 1. M06-optimized structures and ground-state energy ordering for the $Ta(NMe_2)_4[N(SiMe_3)_2]$ stereoisomers. The free energy values are in kcal/mol relative to species **A1**.

Heating $Ta(NMe_2)_4[N(SiMe_3)_2]$ in the absence of a trapping agent gives the imide-bridged dimer $[Ta(NSiMe_3)(NMe_2)_3]_2$ (**D**) and Me_3SiNMe_2 (**C**); the molecular structure of the former product has been established by X-ray diffraction analysis and presumably results from the dimerization of the intermediate imide complex $Ta(NSiMe_3)(NMe_2)_3$ (**B**).[27] DFT analysis of this reaction has confirmed that the α-elimination is a concerted process and is stereospecific, insomuch as only **A2** reacts to give the expected products $Ta(NSiMe_3)(NMe_2)_3$ (**B**) and Me_3SiNMe_2 (**C**). Species **A1** and **A3** do not allow the reacting amido groups to achieve the requisite orientation for the formation of the critical cyclic transition state associated with the transfer of the Me_3Si group to the adjacent Me_2N acceptor ligand. Figure 2 shows the reaction surface for the elimination process and the optimized structures for the **TSA2BC** and **B**. The computed free energy barrier for the reaction is 26.9 kcal/mol, and the barrier for **A1**→**TSA2BC** is in excellent agreement with the experimentally determined $\Delta G^{\neq}$ of 27.1(1.7) kcal/mol. The α-elimination is thermodynamically favored based on an overall ΔG = -7.3 kcal/mol.

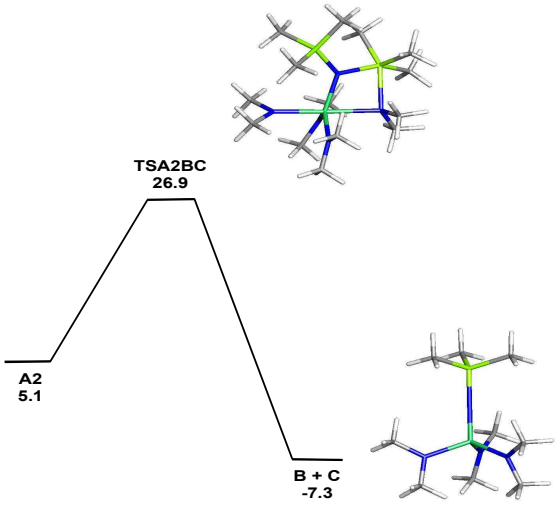

Figure 2. M06-optimized structures and potential energy surface for the α-elimination in **A2** to give **B** and **C**. Energy values are ΔG in kcal/mol with respect to **A1**. The optimized structure for the liberated Me_3SiNMe_2 (species **C**) that accompanies species **B** is not shown.

Dimerization Thermodynamics in $Ta(NR)(NMe_2)_3$ (where R = $SiMe_3$, CMe_3)

In the absence of a trapping agent, $Ta(NSiMe_3)(NMe_2)_3$ (**B**) has been shown to dimerize to **D**. Eq 1 shows the operative equilibrium. The optimized structure of **D**, which is shown below, reveals an excellent correspondence to the reported X-ray diffraction structure. The computed internuclear Ta···Ta distance of 3.191 Å, which is slightly longer (0.028 Å) than that distance found in the solid-state structure,[27] argues against any significant bonding between the two metal centers.[38] The Wiberg index of 0.14 for the Ta-Ta vector in **D** underscores this assertion. As a point of comparison, the benchmark tantalum compounds $(Cp^*Ta)_2B_5H_{11}$ and $Ta_2(PMe_3)_4Cl_4(\mu\text{-}H)_2$,[39] which have been optimized under identical conditions and contain a formal Ta-Ta and Ta=Ta bond, respectively, exhibit Wiberg indices of 0.91 and 2.01. The asymmetry found in the distances of the bridging Ta-N(imide) bonds in the solid-state structure of $[Ta(NSiMe_3)(NMe_2)_3]_2$ are similarly reproduced in the DFT structure using M06 as a functional.

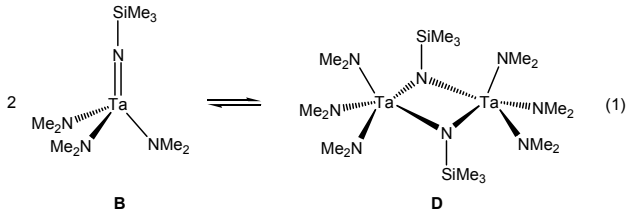

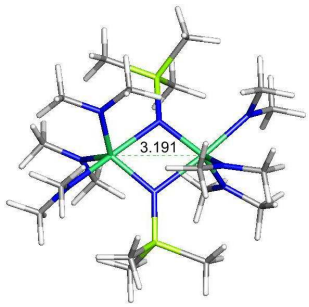

The thermodynamics for the equilibrium depicted in Eq. 1 was computationally evaluated, and the reaction is exergonic with ΔG = -10.3 kcal/mol in accord with the reported experimental data. B3LYP computations failed to model this dimerization accurately and gave a highly endergonic value of ΔG = 29.8 kcal/mol. The M06 computed values of ΔH and ΔS for this reaction are -37.4 kcal/mol and -91 eu, respectively, and these data indicate that **D** is entropically disfavored relative to **B**. The isolation and crystallographic characterization of $[Ta(NSiMe_3)(NMe_2)_3]_2$ (**D**) in the preparative reactions reflect the enthalpic preference for the the dimer vis-à-vis the monomer $Ta(NSiMe_3)(NMe_2)_3$. Other tantalum-based systems that exhibit this monomer-dimer phenomenon include $TaCl_2(NMe_2)_3$ and $Ta(NMe_2)_4(N_3)$.[27,28,38,40]

Closely related to $Ta(NSiMe_3)(NMe_2)_3$ is the well-known Nugent imide derivative $Ta(NCMe_3)(NMe_2)_3$ that exists as a monomer in solution and the solid state.[23,25a,41,42] DFT calculations on $Ta(NCMe_3)(NMe_2)_3$ (monomer and dimer) were performed to better understand the molecularity conundrum in the isostructural $Ta(NEMe_3)(NMe_2)_3$ (where E = C, Si) compounds. The optimized structures of $Ta(NCMe_3)(NMe_2)_3$ and $[Ta(NCMe_3)(NMe_2)_3]_2$ (not shown) are unexceptional compared to the $NSiMe_3$-substituted derivatives **B** and **D**. Dimerization of $Ta(NCMe_3)(NMe_2)_3$ is only slightly unfavorable based on a ΔG = 3.1 kcal/mol, and the computed values for ΔH and ΔS are -24.0 kcal/mol and -91 eu, respectively. Since the entropic contribution to both dimerization reactions is identical, the controlling factor in these two dimerizations rests firmly with the enthalpy. The dimerization of the Si-based imide complex is favored by 13.4 kcal/mol (ΔG) over the analogous C-based imide complex, a feature that we attribute to the larger Si atom and its ability to facilitate the formation of the needed Ta-N(imide) bonds in the dimer. Dimerization of $Ta(NCMe_3)(NMe_2)_3$ is clearly prevented by the smaller tertiary C atom in the imide $NCMe_3$ moiety.

Heterocumulene Trapping of $Ta(NSiMe_3)(NMe_2)_3$

The last phase of this work concerns the trapping of the imide species **B** by the carbodiimide MeN=C=NMe (**E**).[43] Figures 3 and 4 show the optimized structures and free-energy profile for the formation of the mono- and bisguanidinate-substituted products $Ta(NSiMe_3)(NMe_2)_2[MeNC(NMe_2)NMe]$ (**G1**) and $Ta(NSiMe_3)(NMe_2)[MeNC(NMe_2)NMe]_2$ (**I**). The reaction between **B** and MeN=C=NMe (**E**) may be viewed as a pseudo [2+2] cycloaddition process that proceeds by transition state **TSBEF**. Product **F** exhibits a square-pyramidal geometry where the imide group occupies the apical position, and this minimum lies 11.2 kcal/mol below the corresponding reactants **B** and **E**. The coordination of the dimethylamino and amide-nitrogen atoms of the chelate ring to the tantalum atom in **F** confirms the asymmetrical bonding mode of the guanidinate ligand.[44] The conversion of **F** to species **G1** occurs via **TSFG1**, and this transformation is initiated by the opening of the chelate ring in **F** through dissociation of the dimethylamino moiety. Relative to **F**, isomeric **G1** is thermodynamically favored by 6.5 kcal/mol. The optimized structure of **G1** consists of a square pyramid and closely resembles that of **F**, except for the disposition of the symmetrically bound guanidinate ligand.[45]

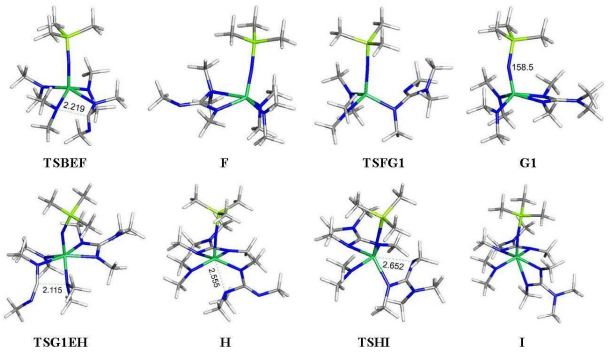

Figure 3. M06-optimized structures for the intermediates **F** through **I** and the corresponding transition states.

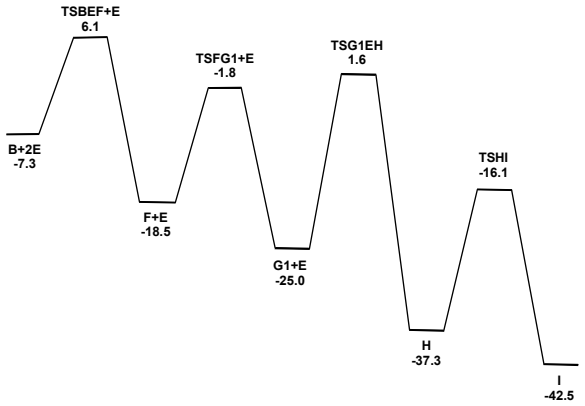

Figure 4. Potential energy surface for the conversion of **B** and **E** (two equivs) to give **I**. Energy values are ΔG in kcal/mol with respect to **A1** + 2**E** → **C** + **I**.

The final guanylation reaction between **G1** and the second equivalent of **E** proceeds by a nucleophilic attack of an amido nitrogen on the central carbon of the carbodiimide ligand, and the transition state **TSG1EH** shows the developing interaction between the participant groups. This is the highest barrier (26.6

kcal/mol) on the guanylation reaction surface and accounts for the observation of both mono- and bisguanidinate-substituted products in those trapping reactions monitored by NMR spectroscopy.[27] The insertion product **H** is nominally six-coordinate and contains an asymmetrically bound guanidinate ligand that exhibits a strong Ta-N(amide) bond and a weaker Ta-N(dimethylamino) bond. The latter moiety is situated pseudo-*trans* to the imide group and reveals an N-Ta-N angle of 155º. The computed Wiberg indices for the Ta-N(amide) and Ta-N(dimethylamino) vectors in the newly formed chelate are 0.65 and 0.23, respectively, confirming the former bond as the stronger of the two in this chelate ring. Wiberg indices of 0.90 and 0.50 were computed for the Ta-N vectors associated with the remaining amido moiety and the average of the two Ta-N bonds in the symmetrically bound guanidinate ligand in **H**. The transformation of **H** to the final product **I** is facilitated by dissociation of the axial dimethylamino group (**TSHI**) and ring closure of the pendant MeN imine moiety in the η^1 guanidinate. Interestingly, in this ring closure the initially coordinated amide moiety ends up *trans* to the imide group. The thermodynamics for the overall reaction (**A1** + **2E** → **C** + **I**) is exergonic with a net energy release of 42.5 kcal/mol.

Conclusions

We have computationally modeled the rare α-elimination in $Ta(NMe_2)_4[N(SiMe_3)_2]$ (**A2**) to give $Ta(NSiMe_3)(NMe_2)_3$ (**B**) and Me_3SiNMe_2 (**C**), and the DFT data are in good agreement with the experimentally determined activation parameters. Among three different $Ta(NMe_2)_4[N(SiMe_3)_2]$ stereoisomers computed by DFT, only the square pyramid with an apical $N(SiMe_3)_2$ group (**A2**) undergoes α-elimination to give $Ta(=NSiMe_3)(NMe_2)_3$ (**B**) and Me_3SiNMe_2 (**C**). The thermodynamics for the monomer-dimer equilibrium involving the imide product $Ta(NSiMe_3)(NMe_2)_3$ (**B**) has been evaluated and found to favor the dimer when the functional M06 is employed. The potential energy surface for the reaction of carbodiimide with $Ta(NSiMe_3)(NMe_2)_3$ (**B**) has been mapped out, and a mechanism involving a cycloaddition-type interaction between a Ta-NMe_2 moiety and the carbodiimide verified.

Acknowledgements

Financial support from the Robert A. Welch Foundation (Grants B-1093-MGR) and National Science Foundation (CHE-0741936 to MGR and CHE-1012173 to ZLX) is much appreciated. We thank Prof. Michael B. Hall (TAMU) for providing us a copy of his *JIMP2* program, which was used to prepare the geometry-optimized structures reported here.

Notes

[*a]Department of Chemistry, The University of North Texas, Denton, Texas 76203, United States. E-mail: cobalt@unt.edu; Tel: +1 940-565-3548.

[b]Department of Chemistry, The University of Tennessee, Knoxville, Tennessee 37996, United States.

† Electronic Supplementary Information (ESI) available: Atomic coordinates of all optimized stationary points and transition states. See DOI: 10.1039/b000000x/

References

1. D. Zarubin, N. Ustynyuk, *Russ. Chem. Rev.,* 2006, **75**, 671.
2. J. F. Berry, *Comments Inorg. Chem.,* 2009, **30**, 28.
3. R. R. Schrock, *Chem. Rev.,* 2009, **109**, 3211.
4. R. Eikey, M. Abu-Omar, *Coord. Chem. Rev.,* 2003, **243**, 83.
5. Y. Li, W. Wong, *Coord. Chem. Rev.,* 2003, **243**, 191.
6. L. Gade, P. Mountford, *Coord. Chem. Rev.,* 2001, **216-217**, 65.
7. W. A. Nugent, J. M. Mayer, *Metal-Ligand Multiple Bonds*, Wiley-Interscience; New York, 1988.
8. D. C. Rosenfeld, P. T. Wolczanski, K. A. Barakat, C. Buda, T. R. Cundari, F. C. Schroeder, E. B. Lobkovsky, *Inorg. Chem.,* 2007, **46**, 9715.
9. P. L. Holland, R. A. Andersen, R. G. Bergman, *Organometallics,* 1998, **17**, 433.
10. S. D. Brown, J. C. Peters, *J. Am. Chem. Soc.,* 2004, **126**, 4538.
11. B. C. Bailey, J. C. Huffman, D. J. Mindiola, W. Weng, O. V. Ozerov, *Organometallics,* 2005, **24**, 1390.
12. E. Kogut, H. L. Wiencko, L. Zhang, D. E. Cordeau, T. H. Warren, *J. Am. Chem. Soc.,* 2005, **127**, 11248.
13. S. C. Bart, E. Lobkovsky, E. Bill, P. J. Chirik, *J. Am. Chem. Soc.,* 2006, **128**, 5302.
14. E. A. Ison, K. A. Abboud, J. M. Boncella, *Organometallics,* 2006, **25**, 1557.
15. M. P. Shaver, M. D. Fryzuk, *J. Am. Chem. Soc.,* 2005, **127**, 500.
16. E. L. Sceats, J. S. Figueroa, C. C. Cummins, N. M. Loening, P. Van der Wel, R. G. Griffin, *Polyhedron,* 2004, **23**, 2751.
17. D. T. Shay, G. P. A. Yap, L. N. Zakharov, A. L. Rheingold, K. H. Theopold, *Angew. Chem. Int. Ed.,* 2005, **44**, 1508.
18. A. O. Chong, K. Oshima, K. B. Sharpless, *J. Am. Chem. Soc.,* 1977, **99**, 3420.
19. E. A. Maatta, B. L. Haymore, R. A. D. Wentworth, *Inorg. Chem.,* 1980, **19**, 1055
20. R. Rossi, A. Marchi, A. Duatti, L. Magon, P. Bernado, *Transition Met. Chem.,* 1985, **10**, 151.
21. U. Burger, U. Wannagat, *Monatsh. Chem.,* 1963, **94**, 761.
22. H. Burger, O. Smrekar, *Monatsh. Chem.,* 1964, **95**, 292.
23. W. A. Nugent, R. L. Harlo, *J. Chem. Soc. Chem. Comm.,* 1978, 579.
24. C. M. Jones, M. E. Lerchen, C. J. Church, B. M. Schomber, N. M. Doherty, *Inorg. Chem.,* 1990, **29,** 1679.
25. Thermolysis of $Ta(NR_2)_5$ (R_2 = Et_2, $^n Pr_2$, $^n Bu_2$, $Me^n Bu$) yields imides $RN=Ta(NR_2)_3$ [R_2 = $Me^n Bu$; $^n BuN=Ta(NMe^n Bu)_3$] as well as $Ta(NR_2)_4$, HNR_2, R-H, and olefins. The formation of the imides here is believed to involve

d[1] $Ta(NR_2)_4$ and NR_2 radicals, see: (a) D. C. Bradley, I. M. Thomas, *Can. J. Chem.,* 1962, **40**, 1355; (b) H. O. Davies, A. C. Jones, E. A. McKinnell, J. Raftery, C. A. Muryn, M. Afzaal, P. O'Brien, *J. Mater. Chem.,* 2006, **16**, 2226; (c) S.-J. Chen, J. Zhang, X. Yu, X. Bu, X. Chen, Z. Xue, *Inorg. Chem.,* 2010, **49**, 4017.

26. W. A. Herrmann, W. Baratta, *J. Organomet. Chem.,* 1996, **506**, 357.

27. B. Sharma, S.-J. Chen, J. K. C. Abbott, X.-T. Chen, Z.-L. Xue, *Inorg. Chem.,* 2012, **51**, 25.

28. S.-J. Chen, H. Cai, Z.-L. Xue, *Organometallics,* 2009**, 28**, 167.

29. M. J. Frisch *et al*., Gaussian 09, Revision E.01, Gaussian, Inc., Wallingford, CT, USA, 2009.

30. (*a*) Y. Zhao, D. G. Truhlar, *Acc. Chem. Res.* 2008, **41**, 157; (*b*) Y. Zhao, D. G. Truhlar, *Theor. Chem. Acc.* 2008, **120**, 215.

31. (*a*) A. D. Becke, *J. Chem. Phys.* 1993, **98**, 5648; (*b*) C. Lee, W. Yang, R. G. Parr, *Phys. Rev. B* 1998, **37**, 785.

32. C. J. Cramer, Essentials of Computational Chemistry, 2nd Ed.; Wiley: Chichester, UK, 2004, p. 378-379.

33. A. E. Reed, L. A. Curtiss, F. Weinhold, *Chem. Rev.,* 1988, **88**, 899.

34. K. B. Wiberg, *Tetrahedron,* 1968, **24**, 1083.

35. (a) JIMP2, version 0.091, a free program for the visualization and manipulation of molecules: M. B. Hall, R. F. Fenske, *Inorg. Chem.,* 1972, **11**, 768. (b) J. Manson, C. E. Webster, M. B. Hall, Texas A&M University, College Station, TX, 2006: http://www.chem.tamu.edu/jimp2/index.html.

36. (a) A. R. Rossi, R. Hoffmann, *Inorg. Chem.,* 1975, **14**, 365; (b) T. D. Westmorelaand, *Inorg. Chim. Acta,* 2008, **361**, 1187.

37. K. F. Purcell, J. C. Kotz, *Inorganic Chemsitry*; W. B. Saunders, Philadelphia, PA, 1977.

38. (a) S.-H. Huang, V. N. Nesterov, M. G. Richmond, *Dalton Trans.,* 2014, **43**, 3453; (b) S.-J. Chen, J. Li, B. A. Dougan, C. A. Steren, X. Wang, X.-T. Chen, Z. Lin, Z.-L. Xue, *Chem. Comm.,* 2011, **47**, 8685.

39. (a) S. K. Bose, K. Geetharani, B. Varghese, S. M. Mobin, S. Ghosh, *Chem. Eur. J.* 2008, **14**, 9058. (b) K. Geetharani, B. S. Krishnamoorthy, S. Kahlal, S. M. Morbin, J.-F. Halet, S. Ghosh, *Inorg. Chem.* 2012, **51**, 10176.

40. M. H. Chisholm, J. C. Huffman, L.-S. Tan, *Inorg. Chem.,* 1981, **20**, 1859.

41. W. A. Nugent, *Inorg. Chem.,* 1983, **22**, 965.

42. For another report on the synthesis of imide-amide Ta(V) derivatives, see: D. C. Bradley, M. H. Gitlitz, *J. Chem. Soc. A,* 1969, 980.

43. The experimentally observed preference of amide over imide reaction in $Ta(NSiMe_3)(NMe_2)_3$ with CyNCNCy agrees with published DFT data on the mixed amide-imide vanadium system $V(NMe)(NMe_2)_2Cl_2$, see: F. Montilla, D. del Río, A. Pastor, A. Galindo, *Organometallics,* 2006, **25**, 4994.

44. For structural reports on asymmetrically bound guanidinates, see: (a) A. M. Mullins, A. P. Duncan, R. G. Bergman, J. Arnold, *Inorg. Chem.,* 2001, **40**, 6952. (b) C. Jones, L. Furness, S. Nembenna, R. P. Rose, S. Aldridge, A. Stasch, *Dalton Trans.,* 2010, **39**, 8788.

45. The guanidinate ligand in **G1** is predicted to be fluxional in solution based on a low-energy torsional twist that affords the less stable trigonal-bipyramidal stereoisomer **G2**. The optimized structures and energies for **TSG1G2** and **G2** are depicted below: